Supplement for: "Constraining the wavefield of volcano-seismic events on Mt. Etna, Italy through rotational sensor and array observations"

Nele I. K. Vesely[1], Eva P. S. Eibl[1], Gilda Currenti[2], Mariangela Sciotto[2], Giuseppe Di Grazia[2], Matthias Ohrnberger[1], Philippe Jousset[3]

[1]Institute of Geosciences, University of Potsdam, Potsdam, Germany
[2]Istituto Nazionale di Geofisica e Vulcanologia-Osservatorio Etneo, Catania, Italy
[3]GFZ Helmholtz Centre for Geosciences, Potsdam, Germany

September 11, 2025

Contents of this file

frequency [1/s]	velocity [m/s]	source depth [m]	uncertainty [m]
0.6	500	510	460.98
0.6	500	600	500.0
0.6	1000	510	651.92
0.6	1000	600	707.11
1.4	500	510	301.78
1.4	500	600	327.33
1.4	1000	510	426.78
1.4	1000	600	462.91

Table S1: Combinations of frequency, velocity and source depth used for the LP location uncertainty calculation.

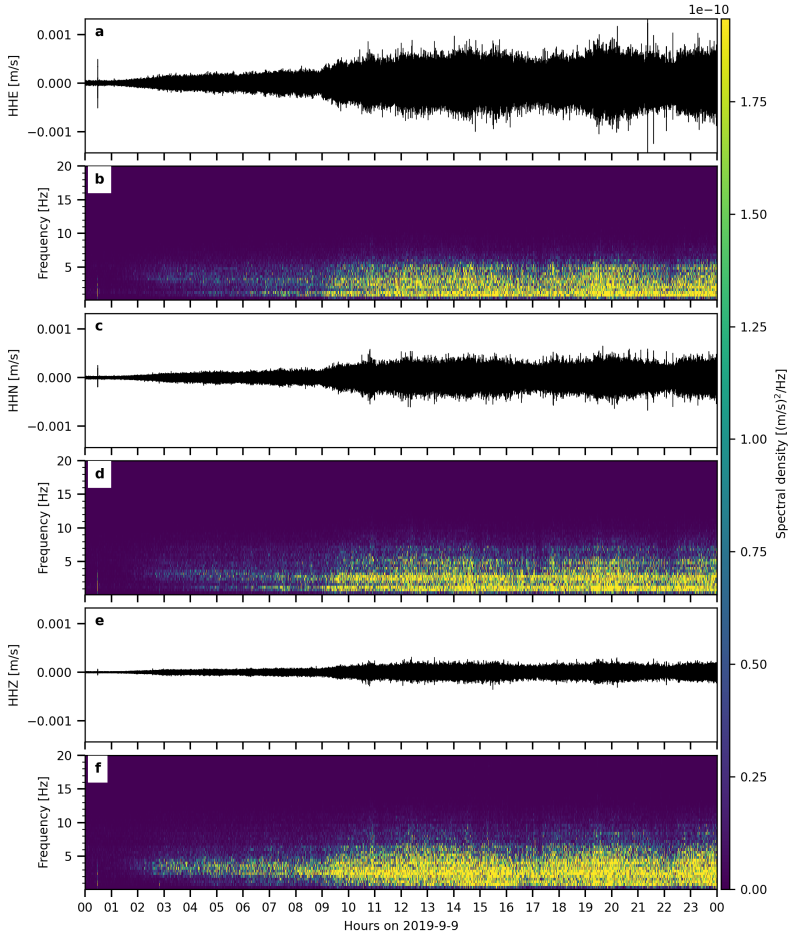

Figure S1: Seismograms and power spectrograms of the strong tremor on 2019-09-09 recorded at the Bb17 seismometer. Filtered from 0.1 to 20 Hz with a sliding window of 500 s and an overlap of 0.25.

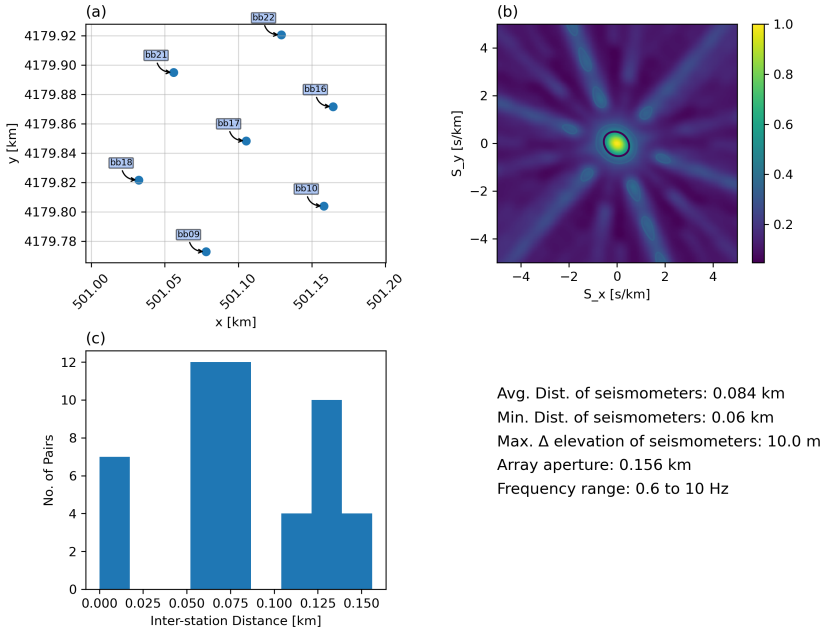

Figure S2: Array response for 0.6 to 10 Hz. (a) Array station set-up. (b) Array response on slowness grid with semblance indicated by color. (c) Inter-station distance distribution.

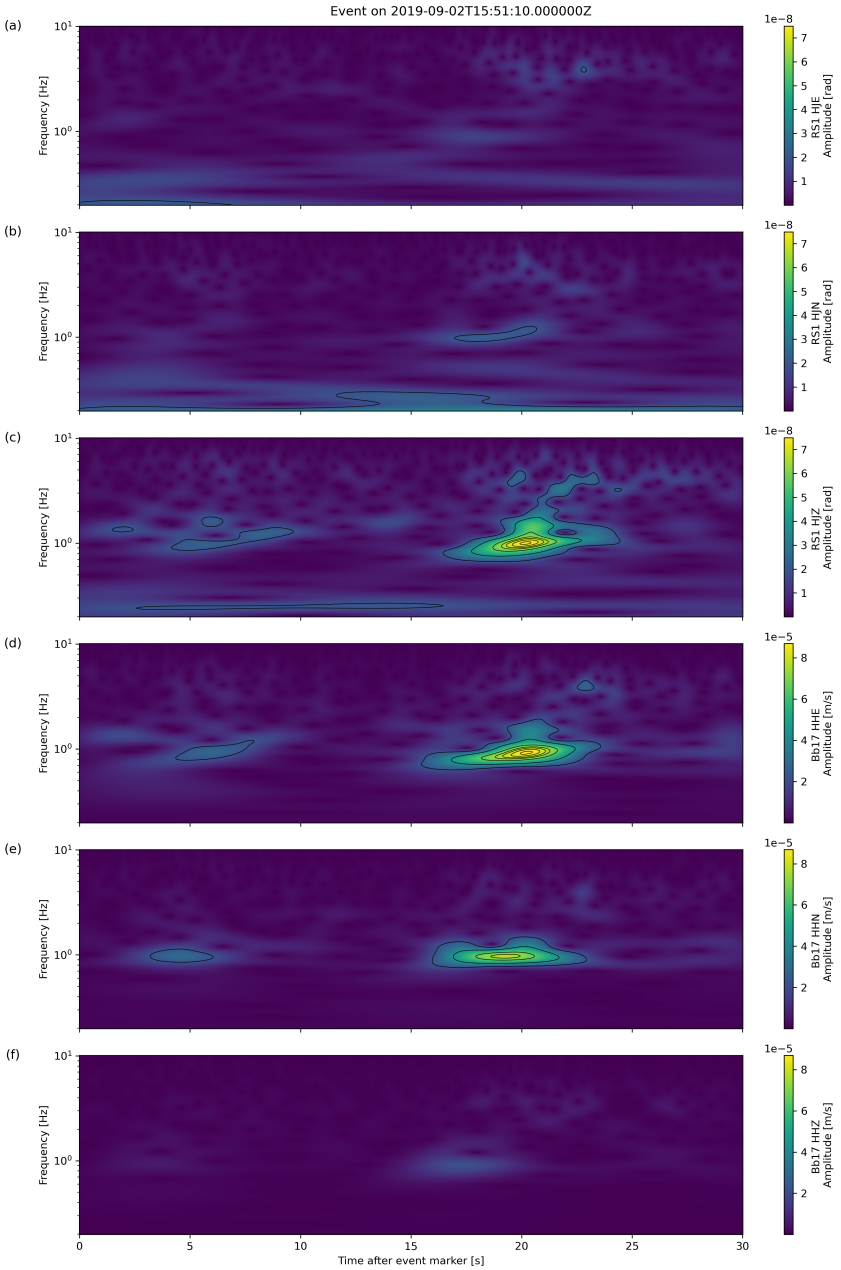

Figure S3: Spectrograms of the LP event on 2019-09-02 15:51 for the seismometer Bb17 and the co-located rotational sensor calculated from corrected and 0.2 to 10 Hz filtered data.

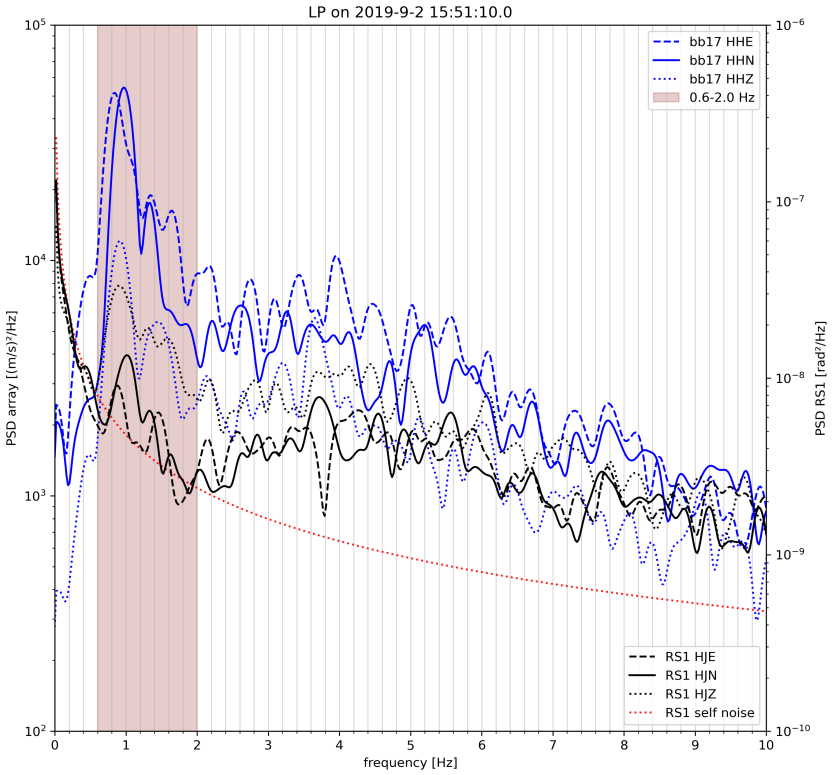

Figure S4: Comparison of power Spectral Densities for all components of Bb17 seismometer and the rotational sensor for the LP event on 2019-09-02 at 15:51:10.

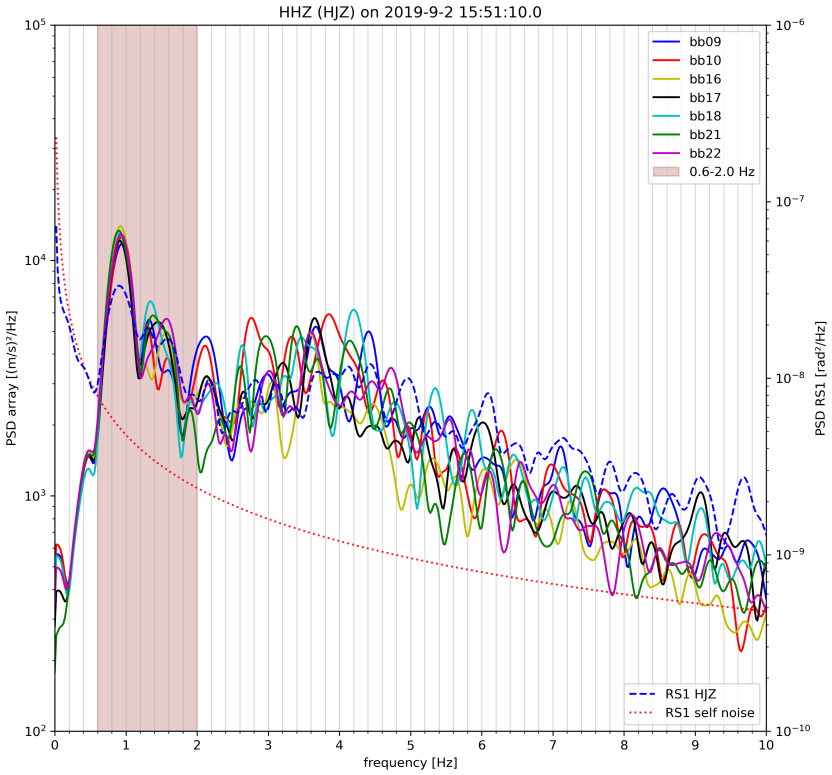

Figure S5: Comparison of power Spectral Densities for the HHZ component from all array seismometers and the rotational sensor component HJZ for the LP event on 2019-09-02 at 15:51:10.

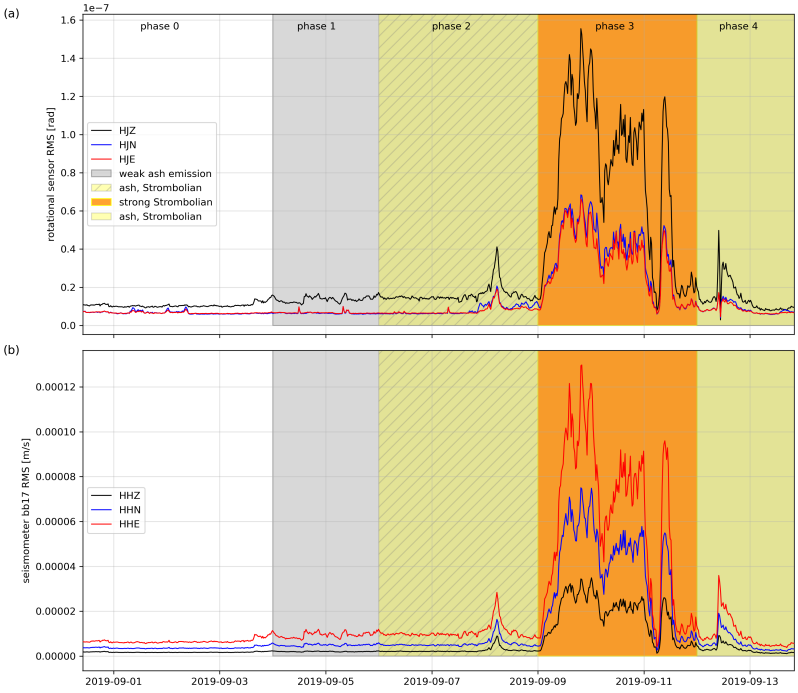

Figure S6: RMS for seismometer Bb17 and rotational sensor RS1 of the tremor signal, filtered from 0.5 to 10 Hz.

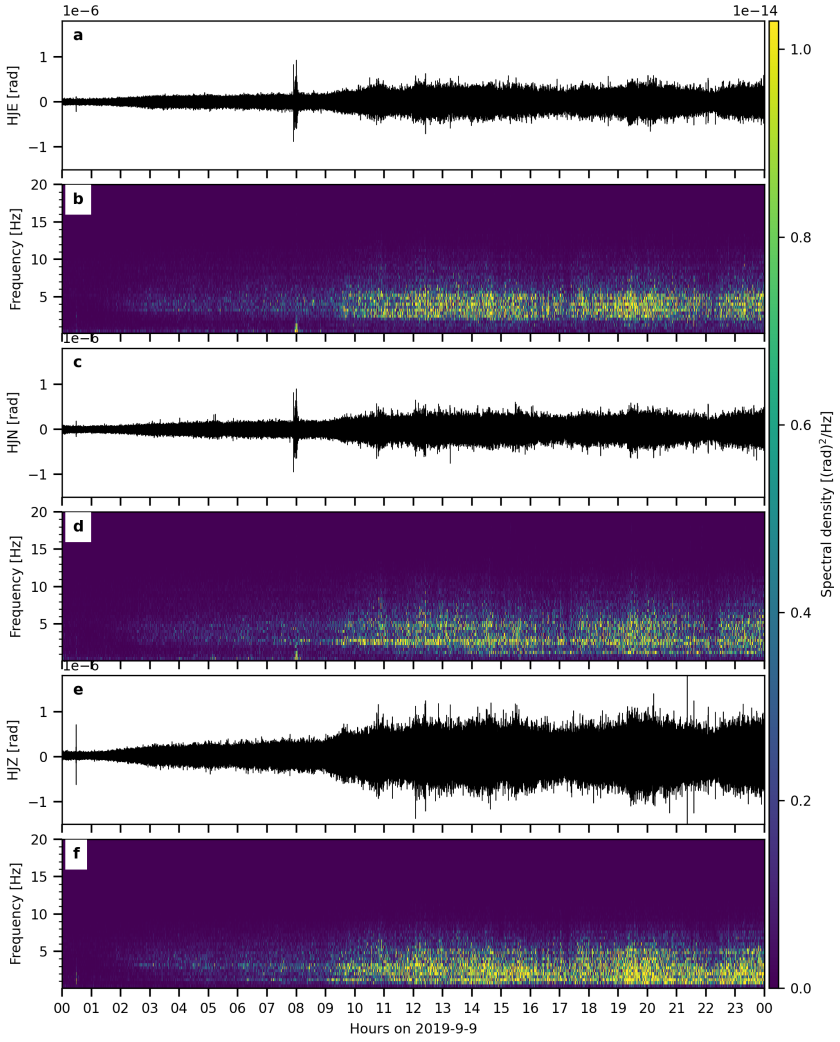

Figure S7: Seismograms and power spectrograms of the strong tremor on 2019-09-09 for the rotational sensor with the same settings as Fig. S1.

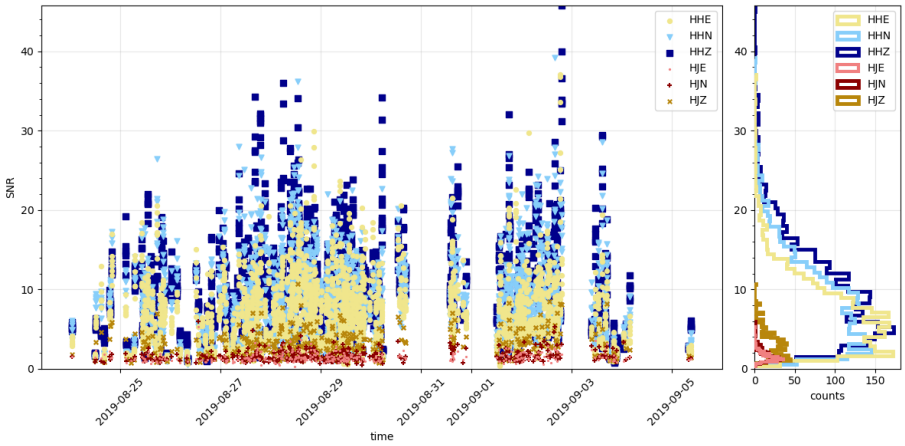

Figure S8: Signal-to-Noise Ratios for all LP events shown in colour according to array components and rotational sensor components.

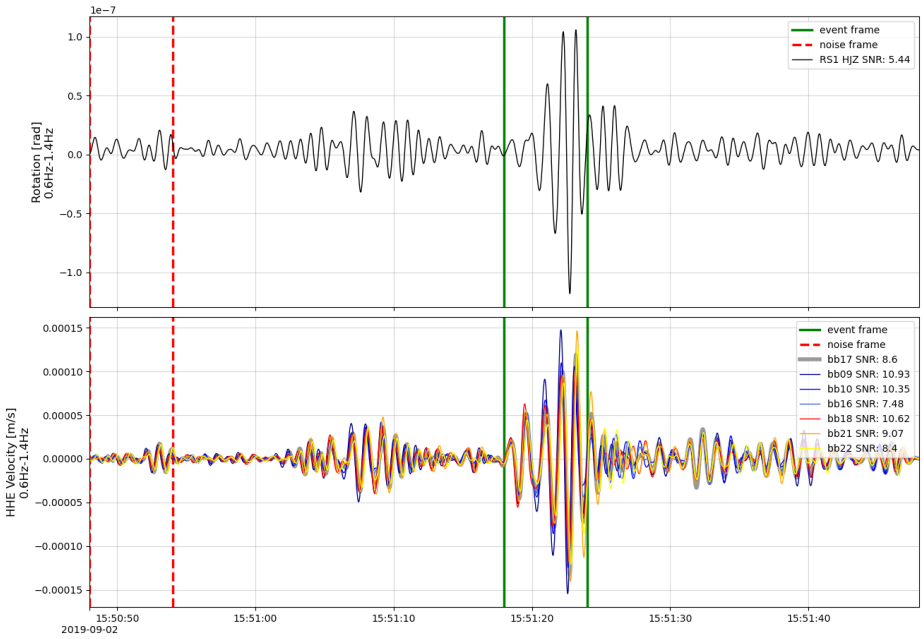

Figure S9: Waveforms of LP event on 2019-09-02 15:51 for the rotational sensor HJZ and the seven HHE components of the array stations. Signal and noise time windows are marked by solid green and red dashed vertical lines, respectively.

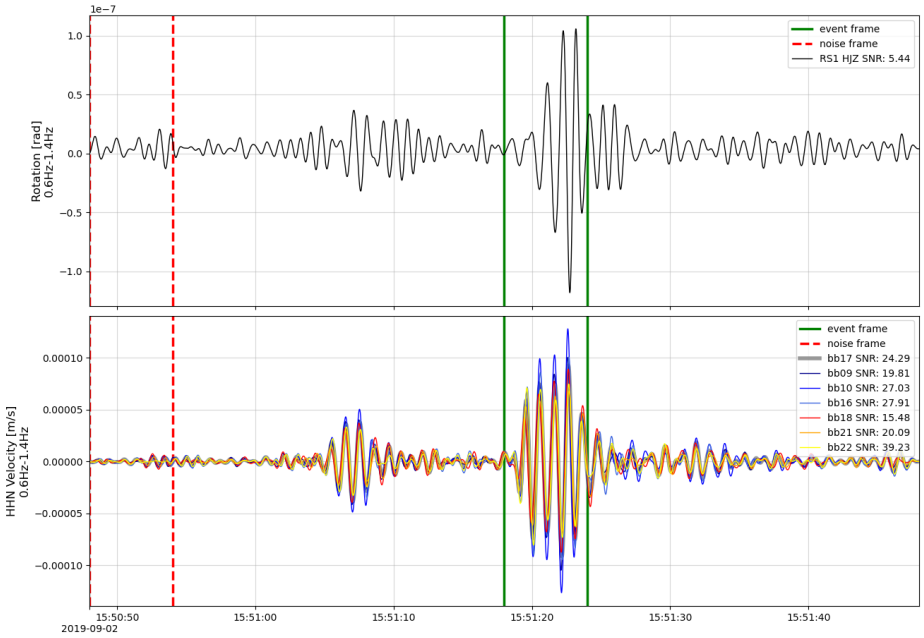

Figure S10: Waveforms of LP event on 2019-09-02 15:51 for the rotational sensor HJZ and the seven HHN components of the array stations. Signal and noise time windows are marked by solid green and red dashed vertical lines, respectively.

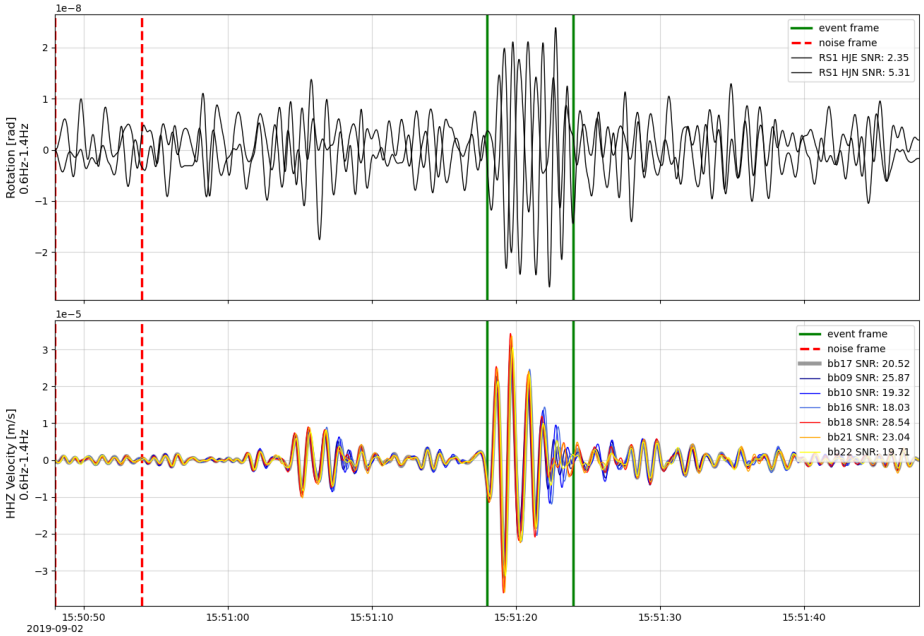

Figure S11: Waveforms of LP event on 2019-09-02 15:51 for the rotational sensor HJE and HJN and the seven HHZ components of the array stations. Signal and noise time windows are marked by solid green and red dashed vertical lines, respectively.

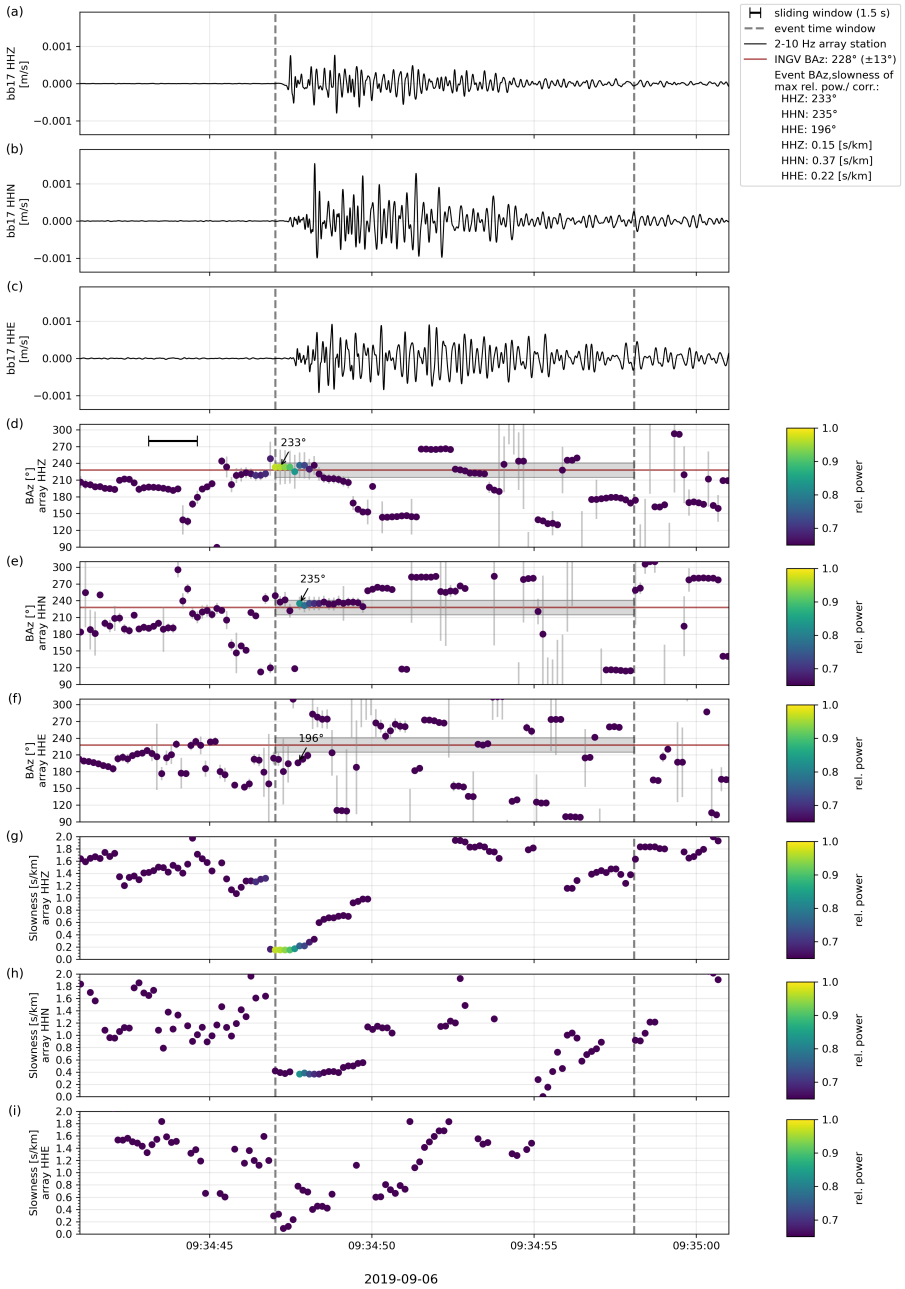

Figure S12: Exemplary VT event on 2019-09-06 09:34. Analysed by array processing for all three seismometer components. (a-c) Waveforms from station Bb17 filtered from 0.2 to 10 Hz. (d-f) Back azimuths obtained from array processing of all the components separately. (g-i) Slowness values from the processing for all three components. Colour indicates relative power.

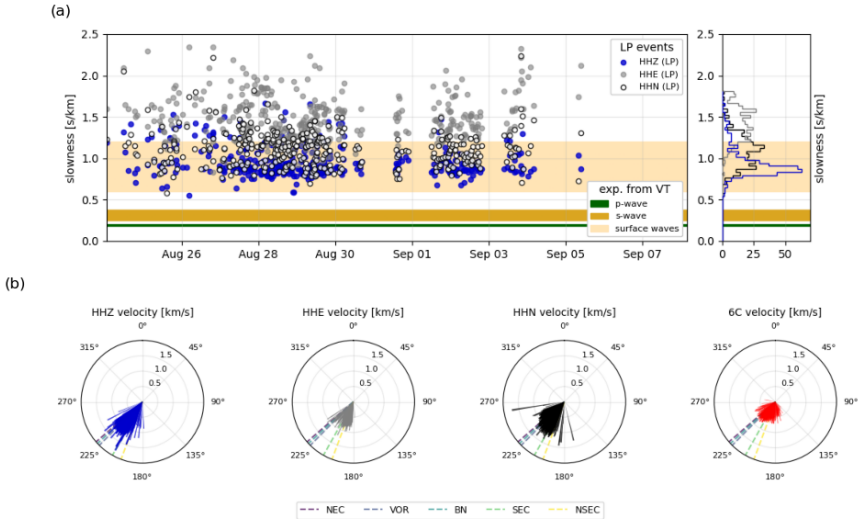

Figure S13: (a) LP event slownesses from the array beamforming of all components with expected wave type slowness ranges from the VT events in coloured plots. (b) Rose plots of directions from inverted slowness results of all array components and the 6C phase velocities.

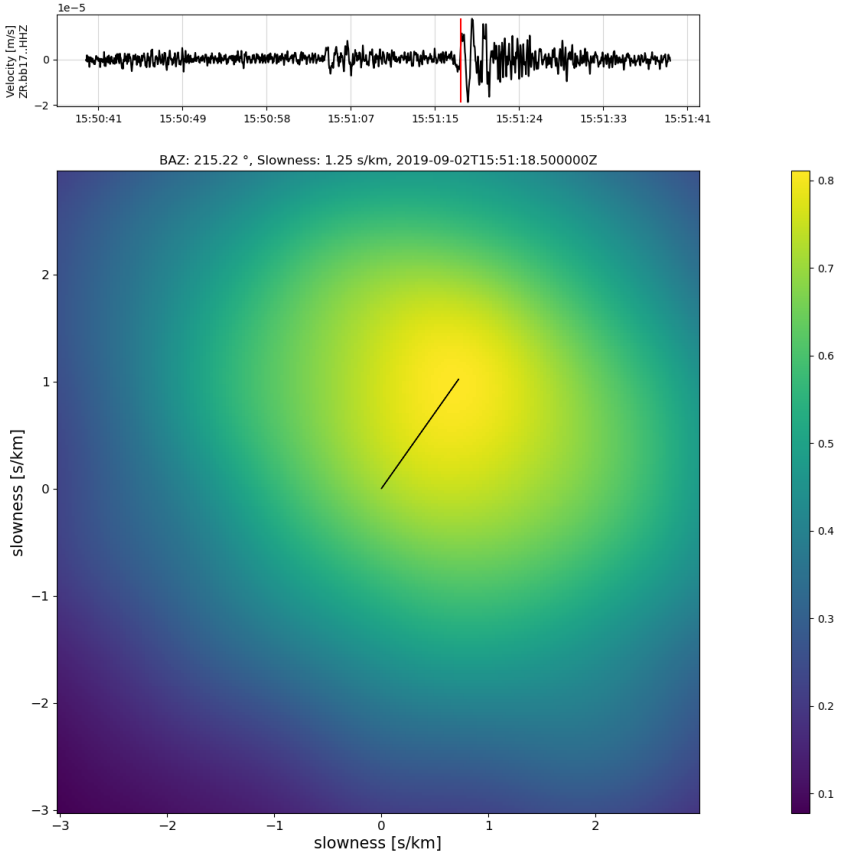

Figure S14: Array response for the LP event with 0.6 to 10 Hz on 2019-09-09 15:51:18.5.